PAM Decomposition of M-ary Multi-h CPM

Erik Perrins, *Member, IEEE,* and Michael Rice, *Senior Member, IEEE*

***Abstract*—It is known that any multilevel continuous phase-modulated (CPM) signal with a *single* modulation index can be exactly represented by a sum of pulse-amplitude modulated (PAM) waveforms. In this paper, we show how multi-h CPM signals can also be represented in this manner. The decomposition is presented in general terms as a function of the alphabet size, modulation indexes, and phase pulse of the CPM scheme. The number of pulses required to exactly construct the signal is shown to increase over that previously given for single-h schemes; this increase is in proportion to the number of modulation indexes. We propose an approximation which significantly reduces the number of signal pulses and which minimizes the mean-squared error for an arbitrary set of modulation indexes. We show that this approximation can have two objectives: 1) to reduce the number of pulses in the same manner as has been proposed for single-h schemes; and/or 2) to reduce the number of multi-h pulses; we also show the conditions where this latter objective is most practical. We compare this minimum mean-squared error approximation with another method which was recently proposed for CPM. We also give numerical results on detection performance which demonstrate the practicality of the proposed approximation.**

***Index Terms*—Continuous phase modulation (CPM), Laurent decomposition, minimum mean-squared error (MMSE) approximation, multi-h CPM, pulse amplitude modulation (PAM).**

I. Introduction

CONTINUOUS phase modulation (CPM) formats are in wide use due to their efficient use of power and bandwidth. Another benefit of CPM is its constant envelope, which is essential when nonlinear amplifiers are used. On the other hand, CPM suffers from high implementation complexity and is difficult to synchronize. These problems are difficult to solve because of the nonlinear nature of the modulation format.

In many instances, the optimal maximum-likelihood detector requires a large bank of correlators [matched filters (MFs)] and a large number of trellis states [1]. A number of approaches have been taken to reduce the trellis size and the number of MFs, e.g., [1]–[3] (see also [4]). One interesting approach is to directly address the nonlinear nature of the signal by decomposing CPM into a linear combination of pulse-amplitude modulated (PAM) components [5]–[7]. Detection schemes have been proposed which are based on this approach [7]–[9] and offer appreciable reductions, both in the number of trellis states and the number of MFs required. The PAM-based approach has also been applied to synchronization problems [7], [9]–[11].

Laurent [5] showed that any binary single-h CPM signal can be exactly represented by a superposition of PAM waveforms

$$s(t;\boldsymbol{\alpha}) = \sum_{k=0}^{Q-1} \sum_{n} b_{k,n} c_k(t - nT). \tag{1}$$

Here, the nonlinearity inherent in CPM is moved to the *pseudosymbols* $b_{k,n}$ (these are obtained from the binary information symbols), which are combined linearly to produce the CPM signal. The set of Q signal pulses $c_k(t)$ are obtained from the phase response of the CPM scheme. An important characteristic of the pulses is that the signal energy is unevenly distributed between them. This is exploited in reduced-complexity detectors [8] which are based on a small subset of these pulses, and require a smaller filter bank and trellis size.

In a subsequent paper, Mengali and Morelli [6] showed that M-ary single-h CPM waveforms (with M even) can also be exactly represented by a PAM decomposition

$$s(t;\boldsymbol{\alpha}) = \sum_{k=0}^{N-1} \sum_{n} a_{k,n} g_k(t - nT). \tag{2}$$

The pseudosymbols and pulses are obtained by viewing the M-ary waveform as a product of P binary waveforms, where P is on the order of $\log_2 M$. Each of these binary waveforms has a PAM representation given by (1) and, by expanding their product, the PAM equivalent of M-ary CPM is given by (2). As with the binary case, the signal energy is unevenly distributed over the pulses which can be exploited in reduced-complexity detectors [9].

Huang and Li [7] considered the special case of single-h CPM formats with integer modulation index (the Laurent decomposition [5] is not valid for this case, though Mengali and Morelli have shown another means of dealing with this limitation [6]). The PAM signal representation in [7] is slightly different from (1) and (2), though reduced-complexity detectors are again obtained by discarding the signal pulses with the smallest amplitudes.

In this paper, we show that any M-ary *multi-h* CPM waveform can be similarly viewed as a superposition of PAM waveforms

$$s(t;\boldsymbol{\alpha}) = \sum_{k=0}^{N-1} \sum_{n} a_{k,n} g_{k,\underline{n}}(t - nT) \tag{3}$$

where the important distinction is that $\{g_{k,\underline{n}}(t)\}$ is a set of $N_h \cdot N$ PAM pulses, N_h being the number of modulation indexes. (While the number $N_h \cdot N$ is an apparent complexity increase over that required for single-h systems [6], in the detector, this is not necessarily the case, since only N MFs are active in

Paper approved by E. Ayanoglu, the Editor for Communication Theory and Coding Applications of the IEEE Communications Society. Manuscript received August 11, 2003; revised August 4, 2004. This work was supported by the T&E S&T Spectrum Efficient Technologies Program under U.S. Air Force Grant DOD ARTM F04700-02-P-0080.

E. Perrins was with the Department of Electrical and Computer Engineering, Brigham Young University, Provo, UT 84602 USA. He is now with the Department of Electrical Engineering and Computer Science, University of Kansas, Lawrence, KS 66045 USA (e-mail: esp@ieee.org).

M. Rice is with the Department of Electrical and Computer Engineering, Brigham Young University, Provo, UT 84602 USA (e-mail: mdr@ee.byu.edu).

Digital Object Identifier 10.1109/TCOMM.2005.860064

any given symbol interval regardless of the number of modulation indexes [12]). We derive a minimum mean-squared error (MMSE) approximation which can be used to reduce this (potentially) large number of signal pulses. The number of pulses can be reduced in two ways: 1) in the same manner as has been proposed for single-h schemes, which is to discard the less significant pulses using an optimal technique; and/or 2) to optimally average the multi-h pulses to produce the equivalent of single-h pulses. Depending on the circumstances, one objective or the other may be of interest, or both can be achieved simultaneously, if so desired. While the second objective is optimal for an arbitrary set of modulation indexes, we show that it is most practical when

$$\max_{0\le n\le N_h-1}\{2^{P-1}h_n\}\le\frac{1}{2} \tag{4}$$

where $\{h_n\}$ are the N_h modulation indexes. The approximation is also practical outside this range when the values of the modulation indexes are close to each other. We compare this MMSE approximation with the method recently proposed in [3], and find that the cited technique yields a closer approximation than the proposed technique in terms of mean-squared error (MSE); however, we also give numerical results on the detection performance of the proposed approximation, which show that it preserves receiver performance to the same degree as the methods in [3]. This result alone establishes the usefulness of the proposed PAM approximation, which has the simultaneous benefit of reducing the required number of trellis states in the detector [8], [12].

The paper proceeds as follows. In Section II, we derive the multi-h PAM representation. We then provide some examples on constructing the signal in Section III. In Section IV, we discuss the autocorrelation of the pseudosymbols, which is used in Section V to derive the MMSE approximation. We give examples on applying the approximation in Section VI, and present conclusions in Section VII.

In what follows, the complex-baseband multi-h CPM signal is given by

$$s(t;\boldsymbol{\alpha})=\exp\{j\psi(t;\boldsymbol{\alpha})\} \tag{5}$$

$$\psi(t;\boldsymbol{\alpha})\triangleq 2\pi\sum_n\alpha_n h_{\underline{n}}q(t-nT) \tag{6}$$

where T is the symbol duration, $h_{\underline{n}}$ are the set of N_h modulation indexes, $\boldsymbol{\alpha}=\{\alpha_n\}$ are the information symbols in the M-ary alphabet $\{\pm1,\pm3,\ldots,\pm(M-1)\}$, and $q(t)$ is the phase pulse. In this paper, the underlined subscript notation in (6) is defined as modulo-N_h, i.e., $\underline{n}\triangleq n \bmod N_h$. The phase pulse $q(t)$ is the integral of the frequency pulse $f(t)$. The frequency pulse is zero outside the time interval (0, LT) and is scaled such that

$$\int_0^{LT}f(\tau)d\tau=q(LT)=\frac{1}{2}. \tag{7}$$

In the numerical examples that follow, we refer to frequency pulses having a rectangular shape of duration L as LREC, and similarly refer to frequency pulses having a raised-cosine shape of duration L as LRC.

II. Derivation of the PAM Representation

We observe that there are at least two approaches one could take to obtain the PAM decomposition of M-ary multi-h CPM. It is clear from (5) that the *multi-h* CPM waveform can be factored into a product of N_h *single-h* waveforms, each with a signaling rate of $1/N_h$ the original system. Mengali and Morelli's approach [6] could then be used to factor the signal yet again into a product of $N_h\times P$ *binary single-h* waveforms. The PAM representation in (1) could then be applied to each waveform, and the expansion of their product would yield the final result. However, Mengali found the product expansion time-consuming for the single-h case, even without the additional complexities introduced by the multi-h case. This approach was not taken here for those reasons. Instead, we first derive the desired multi-h result for the *binary* case. The binary result is then used as a building block for the M-ary case, where we show that Mengali and Morelli's final result can be applied with minor extension. We first discuss some of the characteristics of the binary single-h PAM representation.

A. Binary Single-h Systems

Equation (1) is the superposition of $Q=2^{L-1}$ pulses $c_k(t)$, which are scaled by the pseudosymbols $b_{k,n}$. These are derived from the actual symbols α_n by the nonlinear mapping defined in [5]. The extension of this mapping to the more general multi-h case is trivial, and is given by

$$b_{k,n}=\exp\left\{j\pi\left[\sum_{m=-\infty}^{n}\alpha_m h_{\underline{m}}-\sum_{i=0}^{L-1}\alpha_{n-i}h_{\underline{n-i}}\beta_{k,i}\right]\right\} \tag{8}$$

where $\beta_{k,i}$ is the ith bit in the radix-2 representation of k

$$k=\sum_{i=1}^{L-1}2^{i-1}\beta_{k,i},\quad 0\le k\le Q-1 \tag{9}$$

and $\beta_{k,0}$ is always zero. The structure in (1) is shown in Fig. 1 (ignoring the lower portion of the figure for the moment). The symbols α_n are converted to pseudosymbols and presented at the inputs to a bank of filters with impulse responses $c_k(t)$. The inner sum in (1) represents the pulse train at the output of each of the filters. This picture is helpful in examining the multi-h case.

B. Binary Multi-h Systems

We start by extending the early steps of the derivation in [5] to account for the multi-h case. Laurent showed that when $\alpha_n\in\{\pm1\}$

$$\exp\left\{j2\pi\alpha_n h_{\underline{n}}q(t-nT)\right\}=\frac{\sin\left(\pi h_{\underline{n}}-2\pi h_{\underline{n}}q(t-nT)\right)}{\sin(\pi h_{\underline{n}})}+\exp\{j\pi\alpha_n h_{\underline{n}}\}\frac{\sin\left(2\pi h_{\underline{n}}q(t-nT)\right)}{\sin(\pi h_{\underline{n}})}. \tag{10}$$

We note that (10) is not valid when $h_{\underline{n}}$ is an integer. It was demonstrated in [6] and [7] how this case is handled for single-h CPM schemes; however, it can be argued that this case is of less practical value, since integer modulation indexes have weak

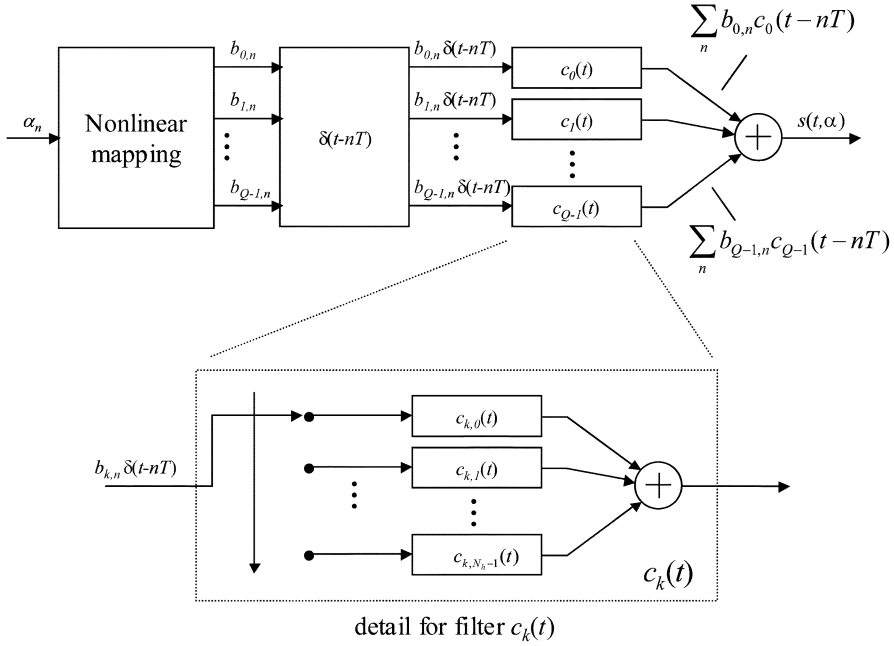

Fig. 1. PAM-based CPM transmitter, including an expanded view of the kth filter.

minimum-distance properties [1]. By inserting (10) into (5) and observing (7), the signal can be expressed as

$$s(t;\boldsymbol{\alpha}) = \exp\left\{j\pi \sum_{m=-\infty}^{\eta-L} \alpha_m h_{\underline{m}}\right\} \prod_{i=0}^{L-1} \Big[u_{i+L,\underline{\eta-i}}(\tau) + \exp\{j\pi\alpha_{\eta-i}h_{\underline{\eta-i}}\}u_{i,\underline{\eta-i}}(\tau)\Big] \quad (11)$$

where $\tau = t \bmod T$, $\eta T \le t < (\eta+1)T$, and the set of functions $u_{j,\underline{i}}(\tau)$ are nonzero in the interval $0 \le \tau < T$ and are defined by

$$u_{j,\underline{i}}(\tau) \triangleq \begin{cases} \frac{\sin\left(2\pi h_{\underline{i}} q(jT+\tau)\right)}{\sin(\pi h_{\underline{i}})}, & 0 \le j \le L-1 \\ \frac{\sin\left(\pi h_{\underline{i}} - 2\pi h_{\underline{i}} q((j-L)T+\tau)\right)}{\sin(\pi h_{\underline{i}})}, & L \le j \le 2L-1 \\ 0, & \text{otherwise.} \end{cases} \quad (12)$$

Expanding the product in (11) yields a sum of 2^L terms. Laurent showed that a number of these terms are similar, and can be grouped into 2^{L-1} pulses of varying lengths.

At this point, a specific example is in order. For convenience, we write $u_{j,\underline{i}}(\tau)$ as $u_{j,\underline{i}}$. When $L = 3$, the product in (11) expands to eight terms

$$\begin{aligned} s(t;\boldsymbol{\alpha}) = {} & b_{0,\eta} \cdot u_{0,\underline{\eta}} \cdot u_{1,\underline{\eta-1}} \cdot u_{2,\underline{\eta-2}} \\ & + b_{0,\eta-1} \cdot u_{1,\underline{\eta-1}} \cdot u_{2,\underline{\eta-2}} \cdot u_{3,\underline{\eta}} \\ & + b_{0,\eta-2} \cdot u_{2,\underline{\eta-2}} \cdot u_{3,\underline{\eta}} \cdot u_{4,\underline{\eta-1}} \\ & + b_{0,\eta-3} \cdot u_{3,\underline{\eta}} \cdot u_{4,\underline{\eta-1}} \cdot u_{5,\underline{\eta-2}} \\ & + b_{1,\eta} \cdot u_{0,\underline{\eta}} \cdot u_{4,\underline{\eta-1}} \cdot u_{2,\underline{\eta-2}} \\ & + b_{1,\eta-1} \cdot u_{1,\underline{\eta-1}} \cdot u_{5,\underline{\eta-2}} \cdot u_{3,\underline{\eta}} \\ & + b_{2,\eta} \cdot u_{0,\underline{\eta}} \cdot u_{1,\underline{\eta-1}} \cdot u_{5,\underline{\eta-2}} \\ & + b_{3,\eta} \cdot u_{0,\underline{\eta}} \cdot u_{4,\underline{\eta-1}} \cdot u_{5,\underline{\eta-2}} \end{aligned} \quad (13)$$

where (8) has been applied. We will focus on the first four terms, which involve the four pseudosymbols $b_{0,n}$ for $n = \eta-3$, $\eta-2$, $\eta-1$, η. For the *single-h* case in (1), these four terms would compose the pulse $c_0(t)$. However, there are two important differences for the *multi-h* case we are considering. The first is that the modulo-N_h index means these terms vary from one symbol time to the next. Thus there is not one pulse, but rather a set of N_h distinct pulses. The second observation is that one of these pseudosymbols, say $b_{0,\eta}$, modulates a pulse for four symbol times. This implies that the terms in (13) at index η are from different pulses and are "interleaved" together. Thus for this $L = 3$ example, the set of pulses described by these four terms are referred to as $c_{0,\underline{n}}(t)$, where the modulo-N_h subscript indexes the distinct pulses in the set. These pulses are given by

$$c_{0,\underline{n}}(t) = \begin{cases} u_{0,\underline{n}}(\tau)u_{1,\underline{n-1}}(\tau)u_{2,\underline{n-2}}(\tau), & 0 \le t < T \\ u_{1,\underline{n+1-1}}(\tau)u_{2,\underline{n+1-2}}(\tau)u_{3,\underline{n+1}}(\tau), & T \le t < 2T \\ u_{2,\underline{n+2-2}}(\tau)u_{3,\underline{n+2}}(\tau)u_{4,\underline{n+2-1}}(\tau), & 2T \le t < 3T \\ u_{3,\underline{n+3}}(\tau)u_{4,\underline{n+3-1}}(\tau)u_{5,\underline{n+3-2}}(\tau), & 3T \le t < 4T \\ 0, & \text{elsewhere} \end{cases} \quad (14)$$

where $\tau = t \bmod T$. The subscript indexes in (14) are left in an unsimplified form to expose the underlying pattern. Since (14) describes one pulse, we note that its length-T segments are not the same as those in (13), which come from multiple pulses "interleaved" together. We can obtain the first four terms in (13) by expanding the summation

$$\sum_n b_{0,n} c_{0,\underline{n}}(t - nT).$$

Additional analysis for this $L = 3$ example produces these same observations for all the pulses in the set $\{c_{k,\underline{n}}(t)\}$. The transmitter in Fig. 1 applies to the multi-h case, with the exception that the pulse filters must be generalized, as shown in the expanded view in the lower portion of the figure. The pseudosymbols are fed into a commutator, which cycles through the set of N_h pulses and "interleaves" the pseudosymbols accordingly. The outputs of all N_h filters are summed to form the final output.

We generalize (14) for all values of L and k to arrive at an expression for the signal pulses

$$c_{k,\underline{n}}(t) = \prod_{j=0}^{L-1} u_{v(k,j,t),w(n,j,t)}(\tau), \quad 0 \le n \le N_h - 1 \tag{15}$$

$$v(k,j,t) \triangleq j + m + L\beta_{k,j} \tag{16}$$

$$w(n,j,t) \triangleq (n + m - (j+m) \bmod L) \bmod N_h \tag{17}$$

$$\tau = t \bmod T, \quad m = \left\lfloor \frac{t}{T} \right\rfloor. \tag{18}$$

The index $v(k,j,t)$ was originally reported by Laurent [5]. For the special case of single-h ($N_h = 1$), the index $w(n,j,t)$ is always zero and may be disregarded, which reduces (15) to the expression reported by Laurent [5]. The pulses have a duration of

$$D_k = \min_i \{L(2 - \beta_{k,i}) - i\}, \quad 0 \le i \le L-1$$

which is unchanged from that in [5]. The binary multi-h signal can be expressed as

$$s(t;\boldsymbol{\alpha}) = \sum_{k=0}^{Q-1} \sum_n b_{k,n} c_{k,\underline{n}}(t - nT). \tag{19}$$

C. M-ary Multi-h Systems

Mengali and Morelli [6] showed that an M-ary CPM signal can be represented as the product of P binary CPM waveforms, where the integer P satisfies the conditions

$$2^{P-1} < M \le 2^P. \tag{20}$$

This is accomplished by representing $\alpha_n \in \{\pm 1, \pm 3, \ldots, \pm(M-1)\}$ as a set of binary coefficients

$$\alpha_n = \sum_{l=0}^{P-1} 2^l \gamma_{l,n}, \quad \gamma_{l,n} \in \{\pm 1\}. \tag{21}$$

For example, when $M = 4$, we have $\alpha_n = 2\gamma_{1,n} + \gamma_{0,n}$. The symbol $\alpha = -3$ is represented as $2(-1) - 1$. Similarly, $\alpha_n = 1$ is given by $2(1) - 1$. Inserting (21) into (5) produces

$$s(t;\boldsymbol{\alpha}) = \prod_{l=0}^{P-1} \exp\left\{ j2\pi \sum_i \gamma_{l,i} h_{\underline{i}}^{(l)} q(t - iT) \right\} \tag{22}$$

$$= \prod_{l=0}^{P-1} \sum_{k=0}^{Q-1} \sum_n b_{k,n}^{(l)} c_{k,\underline{n}}^{(l)}(t - nT) \tag{23}$$

where $h_{\underline{i}}^{(l)} = 2^l h_{\underline{i}}$, and (23) is obtained by applying (19) to each of the binary waveforms in (22). The quantities $b_{k,n}^{(l)}$ and $c_{k,\underline{n}}^{(l)}(t)$ are obtained from (8), (12), and (15) by replacing $h_{\underline{i}}$ and $\{\alpha_i\}$ with $h_{\underline{i}}^{(l)}$ and $\{\gamma_{l,i}\}$, respectively.

The final step in the derivation is to evaluate the products in (23). This is a procedure which Mengali and Morelli indicated was time-consuming, and the details were not given in [6]. However, the final result in [6] for the single-h case contains terms of the form $b_{k,n-i}^{(l)} c_k^{(l)}(t + iT)$, where i is some integer. A close inspection of (23) and its counterpart in [6] shows that the only difference is the modulo-N_h index $\underline{n}$ on $c_{k,\underline{n}}^{(l)}(t)$. Taking this additional index into account, it can be shown that Mengali and Morelli's final result can be extended to contain the terms $b_{k,n-i}^{(l)} c_{k,\underline{n-i}}^{(l)}(t + iT)$. This results in

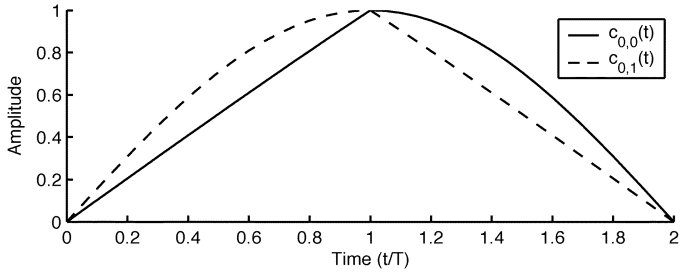

Fig. 2. Signal pulses $c_{0,\underline{0}}(t)$ and $c_{0,\underline{1}}(t)$ for binary 1REC, $h = \{3/8, 4/8\}$.

$$s(t;\boldsymbol{\alpha}) = \sum_{k=0}^{N-1} \sum_n a_{k,n} g_{k,\underline{n}}(t - nT), \quad N = Q^P(2^P - 1) \tag{24}$$

where the pseudosymbols and pulses are obtained by

$$a_{k,n} = \prod_{l=0}^{P-1} b_{d_{j,l}, n - e_{j,l}^{(m)}}^{(l)} \tag{25}$$

$$g_{k,\underline{n}}(t) = \prod_{l=0}^{P-1} c_{d_{j,l}, \underline{n - e_{j,l}^{(m)}}}^{(l)} \left(t + e_{j,l}^{(m)} T \right). \tag{26}$$

The quantities $d_{j,l}$ and $e_{j,l}^{(m)}$ are used exactly as in [6, Sec. III-C], and their lengthy definitions are not reproduced here. Fig. 1 also applies to the signal in (24) with $b_{k,n}$, $c_{k,\underline{n}}(t)$, and Q interchanged with $a_{k,n}$, $g_{k,\underline{n}}(t)$, and N, respectively.

III. Examples

A. Binary Full-Response $2-h$ Systems

We show how to represent binary full-response $2-h$ systems with the PAM decomposition (this is a commonly used example, e.g., [13]). For the moment, we leave the values of the modulation indexes and the phase pulse unspecified. For full-response systems, we have $L = 1$ and $Q = 2^{L-1} = 1$. With $N_h = 2$, we have a total of $2 \cdot 1$ pulses, which we obtain from (15)

$$c_{0,\underline{0}}(t) = u_{0,\underline{0}}(t) + u_{1,\underline{1}}(t - T), \;\; c_{0,\underline{1}}(t) = u_{0,\underline{1}}(t) + u_{1,\underline{0}}(t - T). \tag{27}$$

The signal at index η is given by applying (19)

$$s(t;\boldsymbol{\alpha}) = \sum_{i=\eta-1}^{\eta} b_{0,i} c_{0,\underline{i}}(t - iT), \quad \eta T \le t < (\eta+1)T \tag{28}$$

$$= b_{0,\eta-1} c_{0,\underline{\eta-1}}(\tau + T) + b_{0,\eta} c_{0,\underline{\eta}}(\tau) \tag{29}$$

$$= e^{j\pi \sum_{m=-\infty}^{\eta-1} \alpha_m h_{\underline{m}}} \left[u_{1,\underline{\eta}}(\tau) + \exp\{j\pi \alpha_{\underline{\eta}} h_{\underline{\eta}}\} u_{0,\underline{\eta}}(\tau) \right], \quad \tau = t \bmod T \tag{30}$$

where (30) follows from (27). The form of (30) matches that given by (11).

Fig. 2 shows the two pulses for the 1REC, $h = \{3/8, 4/8\}$ case. A close examination of the two shows that each pulse is itself asymmetric; however, the commutator structure in Fig. 1 "interleaves" the pulses in a manner that produces overall symmetry, as demonstrated in (30).

TABLE I
PSEUDOSYMBOLS, PULSES, AND PULSE LENGTHS FOR 4-ARY $L = 3$ SYSTEM

k	$g_{k,\underline{n}}(t)$	$a_{k,n}$	D_k
0	$c_{0,\underline{n}}^{(0)}(t)c_{0,\underline{n}}^{(1)}(t)$	$b_{0,n}^{(0)}b_{0,n}^{(1)}$	4
1	$c_{0,\underline{n-1}}^{(0)}(t+T)c_{0,\underline{n}}^{(1)}(t)$	$b_{0,n-1}^{(0)}b_{0,n}^{(1)}$	3
2	$c_{0,\underline{n}}^{(0)}(t)c_{0,\underline{n-1}}^{(1)}(t+T)$	$b_{0,n}^{(0)}b_{0,n-1}^{(1)}$	3
3	$c_{0,\underline{n-2}}^{(0)}(t+2T)c_{0,\underline{n}}^{(1)}(t)$	$b_{0,n-2}^{(0)}b_{0,n}^{(1)}$	2
.	.	.	.
.	.	.	.
47	$c_{3,\underline{n}}^{(0)}(t)c_{3,\underline{n}}^{(1)}(t)$	$b_{3,n}^{(0)}b_{3,n}^{(1)}$	1

B. Quaternary 3RC System With $h = \{4/16, 5/16\}$

This example corresponds to the advanced range telemetry (ARTM) CPM waveform [14] which has been adopted by the Range Commanders Council in its IRIG-106 standard [15]. The signal is obtained from the product of $P = \log_2 M = 2$ binary waveforms as in (23), each with a different set of modulation indexes $h^{(0)} = \{4/16, 5/16\}$ and $h^{(1)} = \{8/16, 10/16\}$. The binary systems each consist of $Q = 2^{L-1} = 4$ pairs of pulses. We add the superscript l, $0 \le l \le 1$, to index the lth binary system, i.e., $c_{k,\underline{n}}^{(l)}(t)$. From (15), we obtain

$$\begin{aligned}
c_{0,\underline{n}}^{(l)}(t) &= u_{0,\underline{n}}^{(l)}(t)u_{1,\underline{n-1}}^{(l)}(t)u_{2,\underline{n}}^{(l)}(t) \\
&\quad + u_{1,\underline{n}}^{(l)}(t-T)u_{2,\underline{n-1}}^{(l)}(t-T)u_{3,\underline{n+1}}^{(l)}(t-T) \\
&\quad + u_{2,\underline{n}}^{(l)}(t-2T)u_{3,\underline{n}}^{(l)}(t-2T)u_{4,\underline{n+1}}^{(l)}(t-2T) \\
&\quad + u_{3,\underline{n+1}}^{(l)}(t-3T)u_{4,\underline{n}}^{(l)}(t-3T)u_{5,\underline{n+1}}^{(l)}(t-3T) \\
c_{1,\underline{n}}^{(l)}(t) &= u_{0,\underline{n}}^{(l)}(t)u_{4,\underline{n-1}}^{(l)}(t)u_{2,\underline{n}}^{(l)}(t) \\
&\quad + u_{1,\underline{n}}^{(l)}(t-T)u_{5,\underline{n-1}}^{(l)}(t-T)u_{3,\underline{n+1}}^{(l)}(t-T) \\
c_{2,\underline{n}}^{(l)}(t) &= u_{0,\underline{n}}^{(l)}(t)u_{1,\underline{n-1}}^{(l)}(t)u_{5,\underline{n}}^{(l)}(t) \\
c_{3,\underline{n}}^{(l)}(t) &= u_{0,\underline{n}}^{(l)}(t)u_{4,\underline{n-1}}^{(l)}(t)u_{5,\underline{n}}^{(l)}(t).
\end{aligned} \tag{31}$$

We have already seen $c_{0,\underline{n}}^{(l)}(t)$ in (14), except in the expression above, we have simplified the subscript indexes modulo-2.

When the product of the two binary systems is expanded, there are a total of $N = Q^P(2^P - 1) = 48$ pairs of pulses. Expanding the product involves computing the quantities $d_{j,l}$ and $e_{j,l}^{(m)}$ in (25) and (26). Examples of this procedure are given in [6]. Table I shows a few of the 48 signal components; a complete listing is found in [16].

Fig. 3 shows both sets of 48 signal pulses. As observed by Mengali and Morelli, a 4-ary system has 3 pulses which are most significant [6]. In Fig. 3, there are 9 smaller pulses which are visible, each having a duration of $2T$. The remaining 36 pulses have a duration of T and are not visible.

IV. AUTOCORRELATION OF THE PSEUDOSYMBOLS

Using (8), it can be shown that the autocorrelation function in [5] may be extended to yield

$$B_{k,i}(\underline{n}, q) \triangleq E\left\{b_{k,n}b_{i,n+q}^*\right\} = \prod_{j=0}^{N_h-1} \cos(\pi h_j)^{\Delta(k,i,\underline{n},l,j)} \tag{32}$$

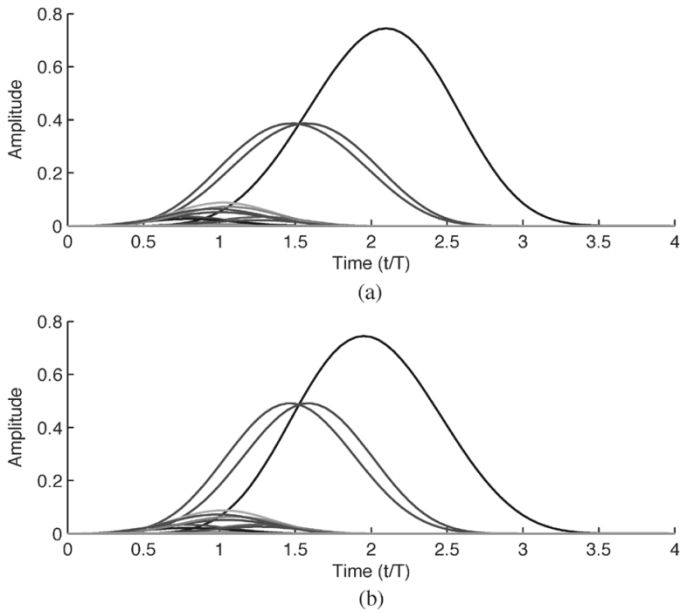

Fig. 3. 48 signal pulses $g_{k,\underline{n}}(t)$ for 4-ary 3RC system with $h = \{4/16, 5/16\}$. (a) n-even. (b) n-odd.

where

$$\begin{aligned}
&\Delta(k,i,\underline{n},l,j) \\
&\quad \triangleq \sum_{m=n+q+1}^{n} \delta_{\underline{m},j} + \sum_{m=n+1}^{n+q} \delta_{\underline{m},j} \\
&\qquad + \sum_{m=0}^{L-1} \delta_{\underline{n-m},j}\beta_{k,m} + \sum_{m=0}^{L-1} \delta_{\underline{n+q-m},j}\beta_{i,m} - 2 \\
&\qquad \times \left[\sum_{m=0}^{\min(L-1,-q-1)} \delta_{\underline{n-m},j}\beta_{k,m} \right. \\
&\qquad\quad + \sum_{m=0}^{\min(L-1,q-1)} \delta_{\underline{n+q-m},j}\beta_{i,m} \\
&\qquad\quad \left. + \sum_{m=\max(0,1-q)}^{\min(L-1,L-q-1)} \delta_{\underline{n-m},j}\beta_{k,m}\beta_{i,m+q} \right].
\end{aligned} \tag{33}$$

Computing the autocorrelation amounts to counting the terms in the exponent of the expectation in (32). However, (32) differs from its counterpart in [5] in that these terms must be grouped into those with common values of $h_{\underline{n}}$. The grouping is conveniently performed by the Kronecker delta function $\delta_{\underline{m},j}$ in (33), which sifts out the terms with a common $h_{\underline{n}}$, and is defined as

$$\delta_{\underline{m},j} \triangleq \begin{cases} 1, & (m \bmod N_h) = j \\ 0, & \text{otherwise.} \end{cases} \tag{34}$$

The sequence $b_{k,n}$ is not stationary, since its autocorrelation is a function of both n and q; however, since the dependence on n is modulo-N_h, it is classified as *cyclostationary*. Examples of computing (32) are given in later sections.

For the important special case of (20), where the size of the symbol alphabet is $M = 2^P$, the separate binary data streams in (21) are independent of each other [6]. In this case, (25) implies

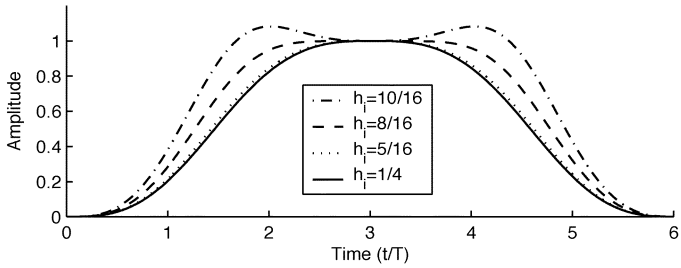

Fig. 4. Functions $u_i(t)$ for 3RC and h_i = 4/16, 5/16, 8/16, and 10/16.

that the autocorrelation of the M-ary pseudosymbols $a_{k,n}$ is the product of P terms of the form

$$B_{k,i}^{(l)}(\underline{n},q)=E\left\{b_{k,n}^{(l)}b_{i,n+q}^{(l)*}\right\},\quad 0\le l\le P-1. \tag{35}$$

The autocorrelation function is an essential part of the mean-square approximation.

V. Mean-Square Approximation

Laurent [5] observed that for the binary single-h case, the signal energy is concentrated mostly in the pulse $c_0(t)$. Mengali and Morelli [6] observed that for the M-ary single-h case, there are $\mathcal{N}_0=2^P-1$ pulses which are most significant, where P is given by (20). These observations have not been proven explicitly, but have been found by numerical observations to apply to most cases.

It has been shown here that the exact multi-h CPM signal can be represented by a sum of $N_h\cdot N$ PAM waveforms, where $N=Q^P(2^P-1)$ and P is given by (20). Fig. 3 shows that for the $L=3$, $M=4$ case, Mengali and Morelli's observation scales for the multi-h case, i.e., there are $N_h\cdot\mathcal{N}_0=2\cdot(2^2-1)=6$ pulses which are most significant. In addition, for the multi-h case, we observe that in many instances, the pulses are similar over the different modulation indexes, as seen in Figs. 2 and 3. These observations suggest two methods for approximating the signal: first by averaging the multi-h pulses to produce the equivalent of single-h pulses; and second by using only the N' most significant pulses (we can select N' to be the number $\mathcal{N}_0$ proposed by Mengali and Morelli or some other value less than N).

An important question is whether averaging the multi-h pulses is practical. Since $\{g_{k,\underline{n}}(t)\}$ are a product of $u_{j,\underline{i}}(t)$, we look to (12) for insight. We observe that $u_{\underline{i}}(t)$ has a fundamentally different shape for $h_i\le 1/2$ than for $h_i>1/2$. This is illustrated in Fig. 4 for the 3RC case with h_i = 4/16, 5/16, 8/16, and 10/16. We see that when $h_i\le 1/2$, $u_i(t)$ is monotonically increasing when $t\le LT$, and monotonically decreasing when $t\ge LT$. This is not true when $h_i>1/2$. This suggests that when

$$\max_{0\le n\le N_h-1}\{2^{P-1}h_n\}\le\frac{1}{2} \tag{36}$$

is satisfied, we can reasonably approximate the $N_h\cdot N$ multi-h pulses with an averaged set of N pulses. We will also show that this averaging approach can also be applied outside this range when the values of the modulation indexes are close to each other. (We again note that averaging the multi-h pulses does not necessarily reduce the matched filtering requirements in the detector, but it does produce an architectural simplification by removing the need for the comutator, etc., in Fig. 1).

The most straightforward approach to this first approximation would be to simply average the multi-h pulses, i.e.,

$$\bar{g}_k(t)\triangleq\frac{1}{N_h}\sum_{j=0}^{N_h-1}g_{k,\underline{j}}(t),\quad 0\le k\le N-1. \tag{37}$$

We would then be left with the problem of reducing the number of pulses from N to N'. Rather than adopting (37), we desire to simultaneously average the multi-h pulses and reduce the overall number of pulses to N', in a manner which best approximates the signal.

We define the approximate signal as

$$\tilde{s}(t;\boldsymbol{\alpha})\triangleq\sum_{k=0}^{N'-1}\sum_{n}a_{k,n}p_k(t-nT),\quad N'\le N \tag{38}$$

where N' is the number of pulses we desire to use, $p_k(t)$ are the signal pulses we wish to obtain, and $a_{k,n}$ are the same as in (24). We desire $\{p_k(t)\}$ to be such that they minimize the normalized MSE between the exact signal in (24) and the approximation in (38), namely

$$\begin{aligned}\tilde{\sigma}^2&\triangleq\frac{\int_0^{N_hT}E\left\{|\tilde{s}(t;\boldsymbol{\alpha})-s(t;\boldsymbol{\alpha})|^2\right\}dt}{\int_0^{N_hT}E\left\{|s(t;\boldsymbol{\alpha})|^2\right\}dt}\\&=\frac{1}{N_hT}\int_0^{N_hT}E\left\{|\tilde{s}(t;\boldsymbol{\alpha})-s(t;\boldsymbol{\alpha})|^2\right\}dt\\&=\frac{1}{N_hT}\sum_{j=0}^{N_h-1}\int_0^{T}E\left\{|\tilde{s}(t+jT,\boldsymbol{\alpha})-s(t+jT,\boldsymbol{\alpha})|^2\right\}dt\end{aligned} \tag{39}$$

where the second line follows from the constant envelope signal model in (5). We follow the approach in [5] and [6], and observe that minimizing (39) is accomplished by minimizing the integrand

$$\sigma^2=\frac{1}{N_hT}\sum_{j=0}^{N_h-1}E\left\{|\tilde{s}(t+jT,\boldsymbol{\alpha})-s(t+jT,\boldsymbol{\alpha})|^2\right\} \tag{40}$$

at each time in the interval $0\le t<T$. For convenience, we let $p_k(n)=p_k(t+nT)$ and $g_{k,\underline{-n}}(t+nT)=g_{k,\underline{-n}}(n)$. We then insert (24) and (38) into (40) and set the derivatives of $p_k(m)$ equal to zero to obtain

$$\begin{aligned}&\sum_{j=0}^{N_h-1}\sum_{i=0}^{N'-1}\sum_{n=0}^{D_i-1}R_{k,i}(\underline{j-m},m-n)p_i(n)\\&\qquad=\sum_{j=0}^{N_h-1}\sum_{i=0}^{N-1}\sum_{n=0}^{D_i-1}R_{k,i}(\underline{j-m},m-n)g_{i,\underline{j-n}}(n)\end{aligned} \tag{41}$$

which describes a set of simultaneous equations for $0\le k\le N'-1$, $0\le m\le D_k-1$, and

$$R_{k,i}(\underline{n},l)\triangleq E\left\{a_{k,n}a_{i,n+l}^*\right\}. \tag{42}$$

For the single-h case, the solution to (41) can be obtained by taking the Fourier transform of both sides [5], [6]. This technique is particularly useful, in that it does not make any assump-

tions about the duration of the pulses obtained in the solution.[1] Fourier techniques cannot be applied in the multi-h case, since the autocorrelation function $R_{k,i}(\underline{n},l)$ is not shift-invariant (i.e., not stationary). The solution is obtained instead through a matrix-vector representation, where we assume $p_k(t)$ has the same duration as $g_{k,\underline{n}}(t)$.

The solution to the set of equations in (41) is

$$\mathbf{P} = \left(\sum_{j=0}^{N_h-1} \mathbf{A}^{(j)}\right)^{-1} \sum_{j=0}^{N_h-1} \left[\mathbf{A}^{(j)}\mathbf{B}^{(j)}\right] \mathbf{G}^{(j)} \tag{43}$$

where the above quantities are defined in the following. We begin by joining the indexes k and m in (41) into a single index $r(k,m)$, and do likewise with i and n to form $c(i,n)$

$$r(k,m) \triangleq m + \sum_{l=0}^{k-1} D_l, \quad c(i,n) \triangleq n + \sum_{l=0}^{i-1} D_l. \tag{44}$$

These indexes both take on values in the range zero to $M^L - 1$. We define the $M^L \times M^L$ matrix $\mathbf{R}^{(j)}$, with rows indexed by $r(k,m)$ and columns indexed by $c(i,n)$. The $(r(k,m),c(i,n))$th entry of $\mathbf{R}^{(j)}$ is given by

$$R^{(j)}_{r(k,m),c(i,n)} \triangleq R_{k,i}(\underline{j-m}, m-n). \tag{45}$$

We note that there are N_h such matrices indexed by j, $0 \le j \le N_h - 1$. It can be shown that $\mathbf{R}^{(j)}$ is symmetric with main diagonal entries $R_{l,l} = 1$. We partition the matrix $\mathbf{R}^{(j)}$ into

$$\mathbf{R}^{(j)} \triangleq \begin{pmatrix} \mathbf{A}^{(j)} & \mathbf{B}^{(j)} \\ \mathbf{C}^{(j)} & \mathbf{D}^{(j)} \end{pmatrix} \tag{46}$$

where $\mathbf{A}^{(j)}$ is square with dimensions $r(N'+1,0) \times c(N'+1,0)$, and $\mathbf{B}^{(j)}$ has dimensions $r(N'+1,0) \times c(N+1,0) - c(N'+1,0)$. The notation $[\mathbf{A}^{(j)}\mathbf{B}^{(j)}]$ in (43) means we concatenate the two partitioned matrices so the resulting matrix has the dimensions $r(N'+1,0) \times c(N+1,0)$.

We define the column vectors $\mathbf{P}$ and $\mathbf{G}^{(j)}$ with the $c(i,n)$th entry as

$$P_{c(i,n)} \triangleq p_i(n), \quad 0 \le i \le N' - 1 \tag{47}$$

$$G^{(j)}_{c(i,n)} \triangleq g_{i,\underline{j-n}}(n), \quad 0 \le i \le N - 1. \tag{48}$$

We emphasize that the vector entries in (47) and (48) are functions of time, which can only be nonzero for $0 \le t < T$. There are N_h vectors $\mathbf{G}^{(j)}$ indexed by j, $0 \le j \le N_h - 1$. This concludes the definitions necessary to compute (43). The solution in (43) minimizes the MSE in (39) for *all* values of modulation indexes, regardless of the condition in (36). This does not mean, however, that the solution in (43) will be useful in all instances.

For cases where (43) produces unsatisfactory results, in particular, those which violate (36), an alternate formulation is to relax the need to average the multi-h pulses. Here we obtain a set of N' pulses for each index n, i.e., a total of $N_h \cdot N'$ pulses. It can be shown that this solution is given by

$$\mathbf{P}^{(j)} = \left(\mathbf{A}^{(j)}\right)^{-1} \left[\mathbf{A}^{(j)}\mathbf{B}^{(j)}\right] \mathbf{G}^{(j)}, \quad 0 \le j \le N_h - 1 \tag{49}$$

$$P^{(j)}_{c(i,n)} = p_{i,\underline{j-n}}(n), \quad 0 \le i \le N' - 1 \tag{50}$$

[1]For the binary case, however, Laurent [5] showed that the pulse $p_0(t)$ obtained in the solution is indeed the same duration as the pulse $c_0(t)$.

where $\mathbf{P}^{(j)}$ is a function of j, $0 \le j \le N_h - 1$, unlike its counterpart in (43). We point out that for the *single-h* case, both (43) and (49) reduce to the same expression. These give the same results as the Fourier approach taken in [5] and [6].

We have shown that the signal can be approximated by reducing the number of terms in an optimal manner along two "dimensions" independently, meaning that we can average the multi-h pulses, or reduce the number of terms from N to N', or do both at once. In general, then, the approximate signal is

$$\tilde{s}(t;\boldsymbol{\alpha}) = \sum_{k=0}^{N'-1} \sum_{n} a_{k,n} p_{k,\underline{n}}(t - nT), \quad N' \le N \tag{51}$$

and for the special case of $p_{k,\underline{n}}(t) = p_k(t)$, it reduces to (38).

We conclude this section by presenting an expression for the residual MSE, which is obtained by inserting (24) and (51) into (39), which yields

$$\tilde{\sigma}^2_{\text{res}} = \frac{1}{N_n T} \sum_{j=0}^{N_h-1} \sum_{k=0}^{N-1} \sum_{i=0}^{N-1} \sum_{m=0}^{D_k-1} \sum_{n=0}^{D_i-1} R_{k,i}(\underline{j-m}, m-n) \times \int_0^T z_{k,\underline{j-m}}(t+mT) z_{i,\underline{j-n}}(t+nT)\,dt$$

where

$$z_{k,\underline{n}}(t) \triangleq \begin{cases} g_{k,\underline{n}}(t) - p_{k,\underline{n}}(t), & 0 \le k \le N' - 1 \\ g_{k,\underline{n}}(t), & \text{otherwise.} \end{cases} \tag{52}$$

Alternatively, if we define the vector

$$\mathbf{Z}^{(j)} \triangleq \mathbf{G}^{(j)} - \begin{pmatrix} \mathbf{P}^{(j)} \\ \mathbf{0} \end{pmatrix} \tag{53}$$

then the residual MSE is

$$\tilde{\sigma}^2_{\text{res}} = \frac{1}{N_n T} \sum_{j=0}^{N_h-1} \sum_{k=0}^{M^L-1} \sum_{i=0}^{M^L-1} \left(\mathbf{R}^{(j)} .* \int_0^T \mathbf{Z}^{(j)} \left(\mathbf{Z}^{(j)}\right)^T dt \right)_{k,i} \tag{54}$$

where the integral is computed on each element in the matrix, and the $*$ operator is defined as an element-by-element multiply.

VI. Examples Using the Approximation

A. Binary Full-Response $2-h$ Systems

We have already shown how this signal is constructed in (30). We now demonstrate how to compute the signal autocorrelation. From (32) and (45), we have

$$\mathbf{R}^{(0)} = \begin{pmatrix} 1 & \cos(\pi h_0) \\ \cos(\pi h_0) & 1 \end{pmatrix}$$
$$\mathbf{R}^{(1)} = \begin{pmatrix} 1 & \cos(\pi h_1) \\ \cos(\pi h_1) & 1 \end{pmatrix} \tag{55}$$

and from (48), we have

$$\mathbf{G}^{(0)} = \begin{pmatrix} g_{0,0}(0) \\ g_{0,1}(1) \end{pmatrix}, \quad \mathbf{G}^{(1)} = \begin{pmatrix} g_{0,1}(0) \\ g_{0,0}(1) \end{pmatrix}. \tag{56}$$

We desire to optimally average the two multi-h pulses to yield one pulse $p_0(t)$. We recognize in this case that $\mathbf{A}^{(j)} = \mathbf{R}^{(j)}$, thus inserting (55) into (43) yields

$$\mathbf{P} = \left(\mathbf{R}^{(0)} + \mathbf{R}^{(1)}\right)^{-1} \left[\mathbf{R}^{(0)}\mathbf{G}^{(0)} + \mathbf{R}^{(1)}\mathbf{G}^{(1)}\right] \tag{57}$$

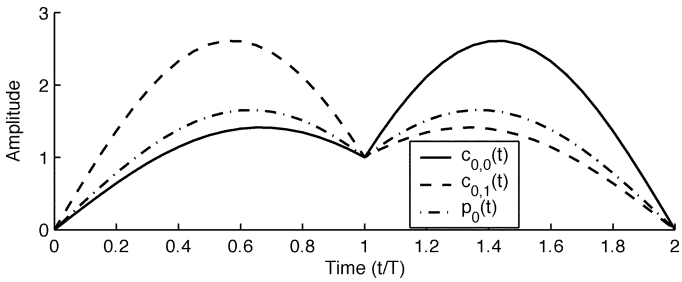

Fig. 5. Signal pulses $c_{0,\underline{0}}(t)$, $c_{0,\underline{1}}(t)$, and $p_0(t)$ for binary 1REC, $h = \{6/8, 7/8\}$.

the computation of which is straightforward for specific values of $h_{\underline{i}}$ and $g_{k,\underline{n}}(t)$. We obtain the pulse $p_0(t)$ from $\mathbf{P}$ according to (47). Fig. 5 shows the two exact pulses and the approximate pulse for the 1REC, $h = \{6/8, 7/8\}$ scheme. The approximate pulse is clearly an average of the two exact pulses; however, these pulses have a fundamentally different shape than those which satisfy the condition (36) (as seen earlier in Fig. 2). We can compute $z_{k,\underline{n}}(t)$ in (52) by letting $p_{0,\underline{n}}(t) = p_0(t)$, which yields the residual MSE

$$\begin{aligned}\tilde{\sigma}^2_{\text{res}} = &\int_0^{2T} z^2_{0,0}(t)dt + \int_0^{2T} z^2_{0,1}(t)dt \\ &+ 2\cos(\pi h_0)\int_0^{T} z_{0,0}(t)z_{0,1}(t+T)dt \\ &+ 2\cos(\pi h_1)\int_0^{T} z_{0,0}(t+T)z_{0,1}(t)dt. \end{aligned} \quad (58)$$

We now compare the results of this optimal approximation with those obtained using the simple average in (37). Fig. 6 shows numerical computations of $\tilde{\sigma}^2_{\text{res}}$ as a function of the two modulation indexes h_0 and h_1 for the 1REC case. Fig. 6(a) is the error when using the MMSE solution $p_0(t)$. Fig. 6(b) is the error when using an averaged pulse $\bar{g}_0(t)$ in (37). There is little difference between the two in the region where both indexes are less than 1/2; however, the optimal approximation greatly outperforms the simple average as the indexes increase beyond 1/2.

The performance measure of greater practical interest is receiver minimum distance, which, together with the number of bit errors per error event and the dependence of the error events on the transmitted data, determines the probability of error performance in additive white Gaussian noise [1, Ch. 2]. The minimum-distance properties of PAM detectors for CPM have been analyzed in [17], which is a special case of the analysis in [18] for the class of mismatched CPM detectors. Applying the final result in [17], Fig. 7 shows the minimum distance *loss* (expressed in decibels) over the $2-h$ plane for the same two approximation cases given in Fig. 6. (The distance data points are taken for $h_0, h_1 \in \{1/16, 2/16, \ldots, 15/16\}$; no information is conveyed by the lines which connect the data points). The first observation from Fig. 7 is that the minimum distance is essentially independent of which approximation is used to average over the multi-h pulses (this not the case for $\tilde{\sigma}^2_{\text{res}}$, as Fig. 6

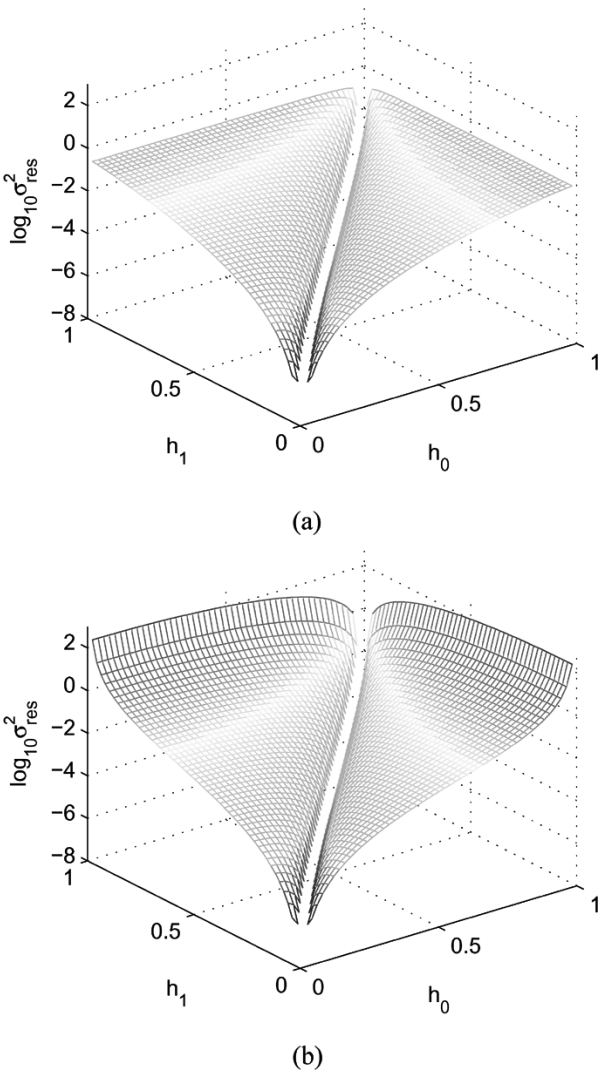

Fig. 6. Binary 1REC system, residual MSE over the $2-h$ plane. (a) $p_0(t)$. (b) $\bar{g}_0(t)$.

clearly shows). The two approximations are never more than 0.1 dB apart over the entire surface shown in Fig. 7, and neither outperforms the other over the entire surface. The second conclusion we draw from Fig. 7 is a general trend of increasing distance loss as the modulation indexes further violate the condition in (36). We also observe that these approximations do better near the line where $h_0 = h_1$ (as is also the case in Fig. 6). This suggests that averaging the multi-h pulses is somewhat practical outside (36) when the modulation indexes are close to each other.

B. Quaternary 3RC System With $h = \{4/16, 5/16\}$

Here each matrix $\mathbf{R}^{(j)}$ is 64×64, with entries given by (45). We show how to compute $R_{1,2}(\underline{n}, q)$, which is one of the autocorrelation functions needed to complete $\mathbf{R}^{(j)}$. From Table I

$$\begin{aligned} R_{1,2}(\underline{n}, q) &= E\left\{b^{(0)}_{0,n-1}b^{(0)}_{0,n+q}b^{(1)}_{0,n}b^{(1)}_{0,n+q-1}\right\} \\ &= E\left\{b^{(0)}_{0,n-1}b^{(0)}_{0,n+q}\right\}E\left\{b^{(1)}_{0,n}b^{(1)}_{0,n+q-1}\right\} \end{aligned} \quad (59)$$

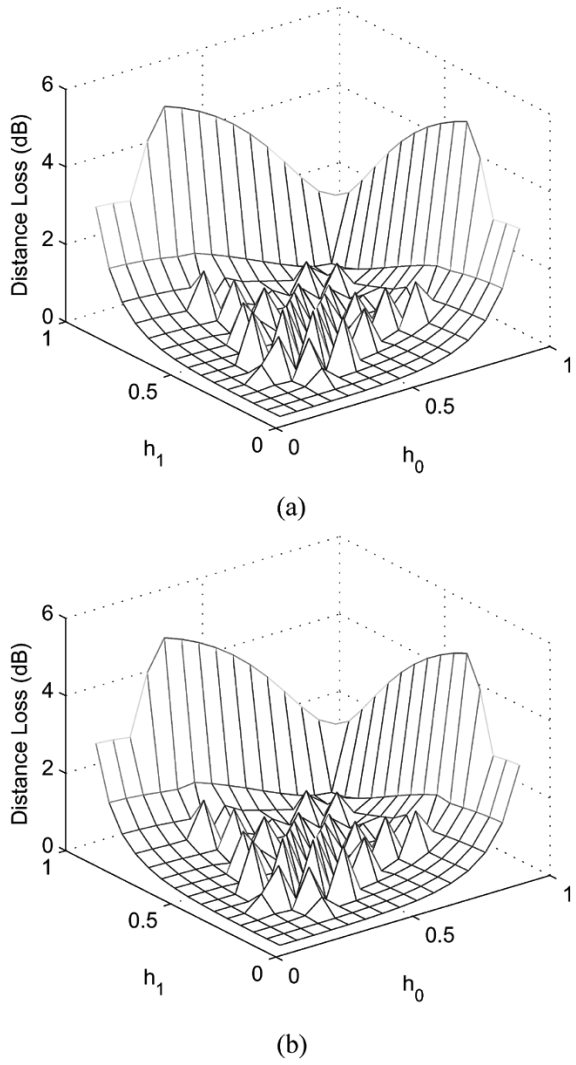

Fig. 7. Binary 1REC system, minimum distance loss (in decibels) over the $2-h$ plane. (a) $p_0(t)$. (b) $\bar{g}_0(t)$.

where we exploit the fact that the pseudosymbols from each of the binary subsystems are independent for $M=4$. We then apply (32) and (33) to each expectation to yield

$$R_{1,2}(\underline{n},q) = \begin{cases} C_0^{(0)}C_1^{(0)}\delta(q-1) \\ \quad +\left(C_0^{(0)}\right)^2 C_1^{(0)}C_1^{(1)}\delta(q-2), & (n \bmod N_h)=0 \\ C_1^{(0)}C_1^{(1)}\delta(q) \\ \quad +C_0^{(0)}C_1^{(0)}\delta(q-1), & (n \bmod N_h)=1 \end{cases} \tag{60}$$

where $C_i^{(l)}=\cos(\pi h_i^{(l)})$ and $\delta(q)$ is unity for $q=0$, and zero otherwise. We note that (60) is zero for all values of q except those shown, because $C_0^{(1)}=\cos(\pi 8/16)=0$.

This CPM scheme is more rich an example than the previous one, in that there are many approximation options one might pursue. Table II gives an assessment of the quality of the approximations that are to be discussed below. We explain the notation in the table using the first entry as an example. The first line corresponds to the exact PAM representation (48×2 pulses of type $g_{k,\underline{n}}(t)$), whose optimal detector has a trellis of 512 states [19]. Since this is the exact representation, there is no residual MSE $\tilde{\sigma}^2_{\rm res}$. The minimum squared distance from [17] is $d'^2_{\rm min}=1.29$, and this is the reference detector for achieving a probability of bit error of $P_b=10^{-5}$. (The minimum distance by itself is not a clear indicator of the overall performance loss for PAM-based CPM detectors, since it is a function of one specific transmitted data sequence, and thus does not dominate the union-bound summation for P_b of practical interest [17]. This is the motivation for quantifying the overall loss at $P_b=10^{-5}$.)

TABLE II
VARIOUS PAM APPROXIMATIONS FOR 4-ARY 3RC SYSTEM WITH $h=\{4/16,5/16\}$

Approximation	States	$\tilde{\sigma}^2_{\rm res}$	$d'^2_{\rm min}$	dB loss at $P_b=10^{-5}$
48×2 ($g_{k,\underline{n}}(t)$)	512	—	1.29	—
3×1 ($p_k(t)$)	32	2.37×10^{-2}	0.30	2.65
3×1 ($\bar{g}_k(t)$)	32	2.52×10^{-2}	0.38	2.19
3×2 ($p_{k,\underline{n}}(t)$)	32	1.17×10^{-2}	0.44	1.61
3×2 ($g_{k,\underline{n}}(t)$)	32	1.39×10^{-2}	0.40	1.89
3×1 (see [19])	128	1.03×10^{-2}	1.07	0.16

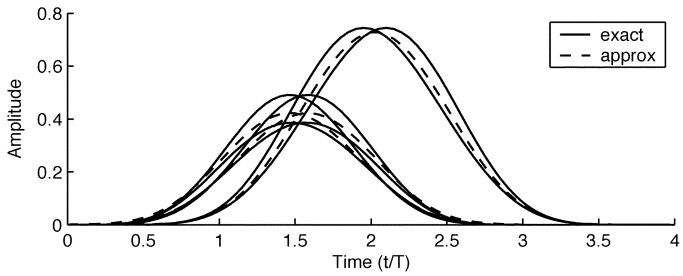

Fig. 8. Three pulses in the approximation $p_0(t)$, $p_1(t)$, and $p_2(t)$ (the three dashed lines), compared with the exact pulses for n-even and n-odd (the six solid lines) for 4-ary 3RC system with $h=\{4/16,5/16\}$.

Since $\mathcal{N}_0=3$, one option is to find the $N'=\mathcal{N}_0=3$ pulses which best approximate the signal. From Table I, we see that the first three pulses have a total of 10 segments of length T. Thus $\mathbf{A}^{(j)}$ are 10×10 matrices, and $\mathbf{B}^{(j)}$ are 10×54 matrices. The solution to (43) is

$$\mathbf{P}=\left(\mathbf{A}^{(0)}+\mathbf{A}^{(1)}\right)^{-1}\left(\left[\mathbf{A}^{(0)}\mathbf{B}^{(0)}\right]\mathbf{G}^{(0)}+\left[\mathbf{A}^{(1)}\mathbf{B}^{(1)}\right]\mathbf{G}^{(1)}\right) \tag{61}$$

which is a 10×1 vector containing the 10 length-T segments of the three pulses $p_0(t)$, $p_1(t)$, and $p_2(t)$. Fig. 8 compares the three pulses in the approximation (dashed curves) with the six exact pulses for even and odd symbol times (solid curves). The second entry in Table II shows that this approximation results in a large reduction in the number of trellis states (a factor of 16), but also a large minimum distance loss (0.30/1.29, or 6.33 dB) and a large overall loss at $P_b=10^{-5}$ (2.65 dB). On the other hand, if the optimal approximation is bypassed and the multi-h pulses are simply averaged and the three largest pulses are retained (i.e., $\bar{g}_0(t)$, $\bar{g}_1(t)$, $\bar{g}_2(t)$), the performance losses are smaller in spite of the increase in $\tilde{\sigma}^2_{\rm res}$ (see the third entry in Table II). This corresponds to an observation in the previous example, where the optimal averaging of the multi-h pulses does not always outperform the simple average in terms of detection performance.

An alternate approximation is to obtain two sets of three pulses, one for even symbol indexes and the other for odd. This solution is given by

$$\mathbf{P}^{(j)} = \left(\mathbf{A}^{(j)}\right)^{-1}\left[\mathbf{A}^{(j)}\mathbf{B}^{(j)}\right]\mathbf{G}^{(j)}, \quad 0 \le j \le 1 \qquad (62)$$

from which we obtain the two sets of three pulses $p_{0,\underline{n}}(t)$, $p_{1,\underline{n}}(t)$, and $p_{2,\underline{n}}(t)$. The fourth and fifth entries in Table II, respectively, correspond to this approximation and the one had by retaining only the 3×2 *original* pulses, $g_{0,\underline{n}}(t)$, $g_{1,\underline{n}}(t)$, and $g_{2,\underline{n}}(t)$. In this case, the optimal approximation outperforms the suboptimal approach by all performance measures considered. This type of approximation (where we reduce the overall number of pulses, but do not average the multi-h pulses) has been considered using other CPM schemes (not shown), and no instances have been found to contradict this finding, though no formal proof of this is given.

In spite of its gains over the other approximations considered so far, the 3×2 optimal approximation is still 1.61 dB inferior to the reference detector. This performance limitation is a direct result of using only using $\mathcal{N}_0$ pulses in the approximation; in fact, this result is not limited to multi-h schemes, since the distance measure in [17] shows a loss of over 2 dB for a similar *single-h* scheme ($M = 4$, 3RC, $h = 1/4$, $N = 48$) when only $\mathcal{N}_0 = 3$ pulses are used. It is clear that an approximation with $\mathcal{N}_0$ pulses is not sufficient to yield near-optimal detection performance for all values of L. A promising approach was given in [12] for the multi-h scheme under consideration, which was: 1) select $N' = 12$ and find the 12×1 best pulses to approximate the signal; 2) average (suboptimally) the two length-$3T$ pulses, and do the same for the nine length-$2T$ pulses (this type of suboptimal averaging was first mentioned in [9]); the end result of these steps is a set of three pulses of durations $4T$, $3T$, and $2T$, respectively. The fifth entry in Table II shows that this configuration performs within 0.16 dB of the reference detector. This hybrid approach demonstrates that near-optimal performance using very few pulses is still available for complex schemes (even when averaging the multi-h pulses).

We conclude this example by comparing the proposed MMSE approximation with the one recently given in [3]. A fair means of comparing the two approaches is not obvious, since the proposed approximation results in real-valued pulses (filters) of various durations, while the approach in [3] produces complex-valued filters of duration T (furthermore, there is no concept of averaging the multi-h filters or a simultaneous reduction in trellis states available in [3]). One possible comparison is in terms of the filtering requirements in the detector, i.e., the required number of real-valued length-T filtering operations. The 3×2 optimal approximation is equivalent to 20 such operations, compared with 5 filters from [3] (using the notation from [3], this is $K = 5$). With $K = 5$, the approximation in [3] achieves $\tilde{\sigma}^2_{\text{res}} = 3.4 \times 10^{-7}$, and essentially no loss in detection performance. Clearly, the method in [3] is superior in terms of performance versus filtering requirements in the detector. However, it cannot be overlooked that the 3×2 optimal approximation also reduces the trellis size by a factor of 16. We can achieve a similar trellis reduction by combining [3] with the methods in [18] or [4], which result in losses of 3.2 or 1.5 dB, respectively. Thus, the approximation in [3] is superior in terms of minimizing the MSE, but the detection performance of the two approximations is nearly identical. This can also be shown for the 128-state trellis configuration in the last entry in Table II and has been confirmed in other CPM schemes (not shown).

VII. Conclusions

We have shown that the PAM representation for CPM can be extended to the M-ary multi-h case. This generalizes previous results, which dealt with the binary and M-ary single-h cases. We have described in general terms a method for computing the pseudosymbols and pulses needed to exactly represent the multi-h signal. These components are a function of alphabet size, modulation indexes, and the phase pulse of the CPM scheme.

We have also shown that the multi-h signal requires a greater number of signal components than an otherwise identical single-h scheme. We have proposed an MMSE approximation which eliminates this increase. This approximation can also be applied to reduce the number of signal components, as previously proposed for single-h systems. We have given examples which illustrate the exact and approximate representations. We have also shown that these approximations, while not always as good in the MMSE sense, yield similar detection performance as existing approximations for CPM.

References

[1] J. B. Anderson, T. Aulin, and C.-E. Sundberg, *Digital Phase Modulation*. New York: Plenum, 1986.

[2] T. Aulin, "Study of a new trellis decoding algorithm and its applications," European Space Agency, Noordwijk, The Netherlands, Final Rep., ESTEC Contract 6039/84/NL/DG, Dec. 1985.

[3] P. Moqvist and T. Aulin, "Orthogonalization by principal components applied to CPM," *IEEE Trans. Commun.*, vol. 51, no. 11, pp. 1838–1845, Nov. 2003.

[4] A. Svensson, "Reduced state sequence detection of partial response continuous phase modulation," *IEE Proc.*, pt. I, vol. 138, pp. 256–268, Aug. 1991.

[5] P. A. Laurent, "Exact and approximate construction of digital phase modulations by superposition of amplitude modulated pulses (AMP)," *IEEE Trans. Commun.*, vol. COM-34, no. 2, pp. 150–160, Feb. 1986.

[6] U. Mengali and M. Morelli, "Decomposition of M-ary CPM signals into PAM waveforms," *IEEE Trans. Inf. Theory*, vol. 41, no. 9, pp. 1265–1275, Sep. 1995.

[7] X. Huang and Y. Li, "The PAM decomposition of CPM signals with integer modulation index," *IEEE Trans. Commun.*, vol. 51, no. 4, pp. 543–546, Apr. 2003.

[8] G. K. Kaleh, "Simple coherent receivers for partial response continuous phase modulation," *IEEE J. Sel. Areas Commun.*, vol. 7, no. 12, pp. 1427–1436, Dec. 1989.

[9] G. Colavolpe and R. Raheli, "Reduced-complexity detection and phase synchronization of CPM signals," *IEEE Trans. Commun.*, vol. 45, no. 9, pp. 1070–1079, Sep. 1997.

[10] G. K. Kaleh, "Differential detection via the Viterbi algorithm for offset modulation and MSK-type signals," *IEEE Trans. Veh. Technol.*, vol. 41, no. 6, pp. 401–406, Nov. 1992.

[11] A. Ginesi, A. N. Andrea, and U. Mengali, "Frequency detectors for CPM signals," *IEEE Trans. Commun.*, vol. 43, no. 2–4, pp. 1828–1837, Feb.–Apr. 1995.

[12] E. Perrins and M. Rice, "Optimal and reduced complexity receivers for M-ary multi-h CPM," in *Proc. IEEE Wireless Commun. Netw. Conf.*, Atlanta, GA, Mar. 2004, pp. 1165–1170.

[13] A. Ginesi, U. Mengali, and M. Morelli, "Symbol and superbaud timing recovery in multi-h continuous phase modulation," *IEEE Trans. Commun.*, vol. 47, no. 5, pp. 664–666, May 1999.

[14] M. Geoghegan, "Description and performance results for a multi-h CPM telemetry waveform," in *Proc. IEEE MILCOM*, vol. 1, Oct. 2000, pp. 353–357.
[15] *IRIG Standard 106-04: Telemetry Standards*, Range Commanders Council Telemetry Group, Range Commanders Council, White Sands Missile Range, NM, 2004.
[16] E. Perrins, "Reduced complexity detection methods for continuous phase modulation," Ph.D. dissertation, Dept. Elect. Comput. Eng., Brigham Young Univ., Provo, UT, 2005.
[17] ——, "A new performance bound for PAM-based CPM detectors," *IEEE Trans. Commun.*, vol. 53, no. 10, pp. 1688–1696, Oct. 2005.
[18] A. Svensson, C.-E. Sundberg, and T. Aulin, "A class of reduced-complexity Viterbi detectors for partial response continuous phase modulation," *IEEE Trans. Commun.*, vol. COM-32, no. 10, pp. 1079–1087, Oct. 1984.
[19] E. Perrins and M. Rice, "Survey of detection methods for ARTM CPM," in *Proc. Int. Telemetering Conf.*, San Diego, CA, Oct. 2004, [CD-ROM].

Erik Perrins (S'96–M'05) received the B.S. (*magna cum laude*), M.S., and Ph.D. degrees from Brigham Young University, Provo, UT, in 1997, 1998, and 2005, respectively.

From 1998 to 2004, he was with Motorola, Inc., Schaumburg, IL, where he was involved with advanced development of land mobile radio products. Since 2004, he has been an industry consultant on receiver design problems such as synchronization and complexity reduction. He joined the faculty of the Department of Electrical Engineering and Computer Science, University of Kansas, Lawrence, in August 2005. His research interests are in digital communication theory, synchronization, channel coding, and complexity reduction in receivers.

Prof. Perrins is a member of the IEEE Communications Society.

Michael Rice (M'82–SM'98) received the B.S.E.E. degree from Louisiana Tech University, Ruston, in 1987 and the Ph.D. degree from the Georgia Institute of Technology, Atlanta, in 1991.

He was with Digital Transmission Systems, Inc., Atlanta, GA, and joined the faculty at Brigham Young University, Provo, UT, in 1991 where he is currently the Jim Abrams Professor with the Department of Electrical and Computer Engineering. He was a NASA/ASEE Summer Faculty Fellow with the Jet Propulsion Laboratory during 1994 and 1995, where he was involved with land mobile satellite systems. During the 1999–2000 academic year, he was a Visiting Scholar with the Communication Systems and Signal Processing Institute, San Diego State University, San Diego, CA. His research interests are in the area of digital communication theory and error control coding, with a special interest in applications to telemetering and software radio design. He has been a consultant to both government and industry on telemetry related issues.

Prof. Rice is a member of the IEEE Communications Society. He was Chair of the Utah Section of the IEEE from 1997 to 1999 and Chair of the Signal Processing and Communications Society Chapter of the Utah Section from 2002 to 2003.